Computational Analysis of the Flowfield of a Mixer-Ejector Nozzle

Yun-Ho Choi*

Mixer-Ejector 노즐 유동장에 관한 수치해석

최 윤호*

ABSTRACT

A time-iterative compressible Navier-Stokes code is developed to analyze the flowfield of a two-dimensional ejector nozzle system. A parametric study has been made for two controlling parameters, duct to nozzle area ratio and nozzle pressure ratio. Results show that there is an optimum area ratio for an efficient pumping of secondary flow. At high area ratios, a freestream flow directly passes through the mixing duct without giving adequate pumping. While at low area ratios, jet boundary is acting as a blockage to incoming flow. The nozzle pressure ratio variation shows that the pumping rate increases as the pressure ratio increases provided there is no interaction between the shroud wall and the shock cell structure.

초 록

본 연구에서는 2차원의 압축성 Navier-Stokes 코드를 개발하여 mixer-ejector 노즐의 유동장 해석을 다양한 덕트와 노즐 면적비 및 노즐 압력비에 대하여 계산을 수행하였다. 덕트와 노즐 면적비 계산에서는 먼저 효율적인 2차 유동의 유입을 위한 최적의 면적비가 있음을 볼 수 있었다. 높은 면적비에서는 입구 자유유동의 적절한 혼합없이 mixing duct를 그대로 통과하는 것을 볼 수 있었고, 낮은 면적비에서는 제트의 경계가 유입 유동에 장애물로 작용하는 것을 볼 수 있었다. 노즐 압력비의 계산에 있어서는 shroud 벽면과 shock cell structure 간에 상호작용이 작다면 유입유량은 압력비에 따라 증가하는 것을 볼 수 있었다.

Key Words : Mixer-Ejector Nozzle, Parametric Study, Nozzle Pressure Ratio, Duct to Nozzle Area Ratio, Compressible Navier-Stokes Code, Shock Cell Structure, Pumping Rate

• 2001년 10월 19일 접수 ~2002년 3월 21일 심사완료

* Ajou University, Department of Mechanical and Industrial Engineering
주연락저자, E-mail : ychoi@ajou.ac.kr, 경기도 수원시 필달구 원천동 산5

1. Introduction

The acoustic challenge to the design of High Speed Civil Transport (HSCT) engines is to reduce noise to FAR 36 stage III noise levels1), while maintaining economic viability of aircraft. In order to meet the above requirement and to provide a high level of performance, the development of a low noise exhaust nozzle design is essential. One of the current, promising technologies is the mixer-ejector concept developed by W. Presz et al.2-4). The mixer-ejector concept introduces an array of large scale, low intensity streamwise vortices into the downstream mixing duct. These vortices enhance mixing through a convective stirring process. This results in increased pumping performance with more completely mixed flows exiting the ejector shroud, which consequently reduces jet exhaust noise.

In the present study as a preliminary step to analyze the flowfield inside the mixer-ejector nozzle, a simplified two-dimensional ejector is considered. A schematic of the two-dimensional ejector nozzle is shown in Fig.1. The ejector is composed of three major components, primary nozzle, secondary inlet, and mixing duct. The secondary flow is drawn from the freestream. The inlet has an elliptical bellmouth to direct the secondary airflow smoothly into the mixing duct. This mixing duct has a diffuser section which lowers the mixing duct pressure to enhance the ejector pumping rate. The diffuser wall angle for the present case is 4 degree. The mixing duct area can be varied by moving the shroud vertically.

The flow feature in the ejector nozzle system is complicated by the strong inviscid/ viscous interaction, freestream entrainment, shock cell structure, and the coexistence of subsonic and supersonic regions. Up to now, most of the analytical studies for ejector nozzle systems are based on Von Karman's control volume approach5,6). It is necessary to use the complete Navier-Stokes equations to analyze the above complex phenomena properly. Deese and Agarwal7) presented numerical solutions of Navier-Stokes equations for ejector flowfields using a Runge-Kutta time stepping method but their results were limited for the subsonic flow regime. In the present study, a time-iterative compressible Navier-Stokes code is developed to investigate the ejector flowfields mainly for underexpanded flows.

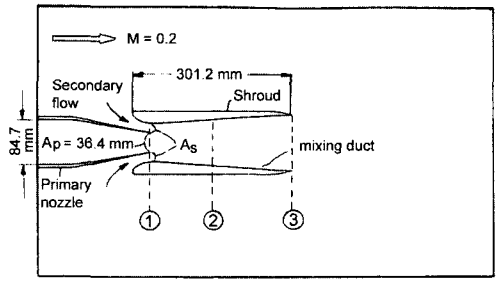

Fig.1 Schematic of two-dimensional ejector nozzle

It has been known that the features of the ejector flow depend on several parameters such as geometry of the mixing duct, duct to nozzle area ratio, duct length to width ratio, primary nozzle location with respect to the inlet of mixing duct, primary jet pressure and Reynolds number etc. In the present study, the two controlling parameters, duct to nozzle area ratio (AR) and nozzle pressure ratio (NPR) are chosen and a parametric study has

been made to study their effects on the ejector flowfield. Computational results are also compared with experimental results in order to validate the code.

2. Governing Equations

The flow through the ejector nozzle can be described by the compressible Navier-Stokes equations. The nondimensional form of the equations can be written in the strong conservation-law form and in the generalized coordinate system as follows:

$$\frac{\partial Q}{\partial t} + \frac{\partial E}{\partial \xi} + \frac{\partial F}{\partial \eta} = \frac{1}{Re}\left(\frac{\partial V_{\xi}}{\partial \xi} + \frac{\partial V_{\eta}}{\partial \eta}\right) \tag{1}$$

where, Q is the primary dependent vector and the vectors, E and F represent inviscid flux vectors:

$$Q = \frac{1}{J}\begin{bmatrix} \rho \\ \rho u \\ \rho v \\ e \end{bmatrix}$$

$$E = \frac{1}{J}\begin{bmatrix} \rho U \\ \rho u U + \xi_x p \\ \rho v U + \xi_y p \\ (e+p)U \end{bmatrix} \quad F = \frac{1}{J}\begin{bmatrix} \rho V \\ \rho u V + \eta_x p \\ \rho v V + \eta_y p \\ (e+p)V \end{bmatrix} \tag{2}$$

In these expressions, x and y represent the cartesian coordinates, and ξ and η are the transformed coordinates. The quantity J is the Jacobian of the transformation defined as $\partial(\xi,\eta)/\partial(x,y)$. The variables ρ and p denote density and static pressure, u and v are velocity components in cartesian coordinates, e is the total energy per volume defined as $\rho\{\varepsilon + (u^2+v^2)/2\}$ where ε is the internal energy. The quantities U and V are the contravariant velocities defined as

$$U = \xi_x u + \xi_y v \ , \quad V = \eta_x u + \eta_y v \tag{3}$$

On the right hand side of Eq.(1), the vectors V_{ξ} and V_{η} represent viscous flux vectors composed of linear combination of V_x and V_y which are the cartesian components of viscous flux vectors:

$$\begin{aligned} V_{\xi} &= (\xi_x V_x + \xi_y V_y)/J \\ V_{\eta} &= (\eta_x V_x + \eta_y V_y)/J \end{aligned} \tag{4}$$

The cartesian viscous vectors V_x and V_y are

$$V_x = \begin{bmatrix} 0 \\ \tau_{xx} \\ \tau_{xy} \\ u\tau_{xx} + v\tau_{xy} - \dfrac{k}{(\gamma-1)Pr}\dfrac{\partial T}{\partial x} \end{bmatrix}$$

$$V_y = \begin{bmatrix} 0 \\ \tau_{xy} \\ \tau_{yy} \\ u\tau_{xy} + v\tau_{yy} - \dfrac{k}{(\gamma-1)Pr}\dfrac{\partial T}{\partial y} \end{bmatrix} \tag{5}$$

where the components of the shear stress tensor are given by

$$\begin{aligned} \tau_{xx} &= (\lambda+2\mu)\frac{\partial u}{\partial x} + \lambda\frac{\partial v}{\partial y} \\ \tau_{yy} &= (\lambda+2\mu)\frac{\partial v}{\partial y} + \lambda\frac{\partial u}{\partial x} \\ \tau_{xy} &= \mu\left(\frac{\partial u}{\partial y} + \frac{\partial v}{\partial x}\right) \end{aligned} \tag{6}$$

Here μ is the viscosity, k is the thermal conductivity, and λ is the second coefficient of viscosity. The Re and Pr are the Reynolds number and Prandtl number, respectively. For the present study, the properties μ is evaluated by the Sutherland formula as

$$\frac{\mu}{\mu_0}=\left(\frac{T}{T_0}\right)^{3/2}\frac{T_0+T_s}{T+T_s} \tag{7}$$

where T_s is the Sutherland temperature constant. The Navier-Stokes equations are augmented by the equation of state taken here as that of a perfect gas. Thus, the total energy is defined by

$$e=\frac{p}{\gamma-1}+\rho\left(\frac{u^2+v^2}{2}\right) \tag{8}$$

where γ is the ratio of specific heats.

For the turbulence calculations, the algebraic turbulence model based on the Baldwin and Lomax8) formulation is employed for the eddy viscosity.

3. Numerical Procedure

The numerical method used to solve Eq.(1) employs an Euler implicit discretization in time along with central differencing in space for both the inviscid and viscous terms. Efficient solution of the resulting matrix can be obtained by using the approximate factorization with diagonalization of the inviscid terms9). Thus the diagonal form of the factored algorithm is

$$T_1\left(I+\Delta t\frac{\partial \Lambda_1}{\partial \xi}\right)N_{12}\left(I+\Delta t\frac{\partial \Lambda_2}{\partial \eta}\right)T_2^{-1}\Delta Q=RHS \tag{9}$$

where RHS is the residual of steady state version of Eq.(1).

$$RHS=-\Delta t\left[\left(\frac{\partial E^n}{\partial \xi}+\frac{\partial F^n}{\partial \eta}\right)-\frac{1}{Re}\left(\frac{\partial V_\xi}{\partial \xi}+\frac{\partial V_\eta}{\partial \eta}\right)\right] \tag{10}$$

Here Λ_i(i=1-2) are eigenvalue matrices of the Jacobians of flux vectors E and F. T_i(i=1-2) are the matrices of right eigenvectors and N_{12} is $T_1^{-1}T_2$. In addition, Jameson's type of artificial dissipation10) is added to the RHS for monotonocity and stability. The above procedure results in the scalar tridiagonal matrix which can be inverted in an efficient manner. All equations are solved simultaneously at each time step until convergence to a steady state is reached.

4. Boundary Conditions

The flow domain of interest is shown in Fig.1. In the present study, we compute only half of this domain since the flowfield is symmetric. Boundary conditions are specified at the upstream and downstream ends, at the farfield, and on all walls. At the upstream boundary stagnation pressure, stagnation temperature and flow angle (v/u) of the incoming stream are specified. These three boundary conditions are augmented by extrapolating the left running Riemann invariant. The flowfield at the downstream end is mixed subsonic/supersonic. For the supersonic flow region, since no physical boundary condition is needed, all flow variables are extrapolated. For the subsonic flow region, back pressure is specified for a given freestream Mach number. The no slip condition and thermally adiabatic conditions are imposed on all walls. This condition is again augmented by the normal momentum equation. At the nozzle exit and at the trailing edge of the shroud, a Kutta condition is imposed to ensure the continuity of

pressure on both sides of the wall:

$$\frac{\partial p}{\partial n}\Big|_{lower} = \frac{\partial p}{\partial n}\Big|_{upper}, \quad p_{lower} = p_{upper} \quad (11)$$

The farfield boundary condition for the present case uses normal velocity v=0, and the remaining flow variables are extrapolated. A symmetry condition is imposed on the plane of symmetry of the computational domain.

5. Results and Discussion

To understand the physical flow phenomena in the ejector nozzle system, a parametric study has been made for two controlling parameters, mixing duct to nozzle area ratio (AR) and nozzle pressure ratios (NPR). Herein, AR is defined as the ratio of the mixing duct inlet area (As) to the primary nozzle throat area (Ap) (AR=As/Ap, refer to Fig.1). The width at locations 1, 2, 3 depends on the area ratios(AR). For AR=1.0, these are 36.4, 81.9, 97.1mm respectively. The divergence angle of mixing duct exit is 4 degree. All calculations are performed on a 171 x 91 grid. The typical grid used for the present calculations is shown in Fig.2. Grid is clustered near all walls and at the nozzle exit to resolve boundary layer and rapid expansion of the flow. The farfield boundary is located about five widths of mixing duct from the shroud so that wall effects may be negligible. In all calculations, freestream Mach number of 0.2 is used to simulate take-off conditions and the flow angle at the upstream end is v/u=0.

Figure 3 shows results for AR's ranging from 1 to 6. Varying the area ratio was accomplished by moving the shroud wall vertically relative to the centerline. Figure 3 shows Mach number and pressure contours for the different area ratios at a nozzle stagnation pressure of 3.5 atm and an ambient stagnation pressure of 1 atm, which corresponds to an NPR of 3.5. The nozzle stagnation temperature is 505 K, and the ambient stagnation temperature is 300 K. In all calculations, Reynolds, Prandtl and turbulent Prandtl numbers used are 1.3×10^7, 0.72, and 0.9, respectively. The Reynolds number is based on the nozzle width and nozzle exit velocity which would be obtained for an isentropic expansion.

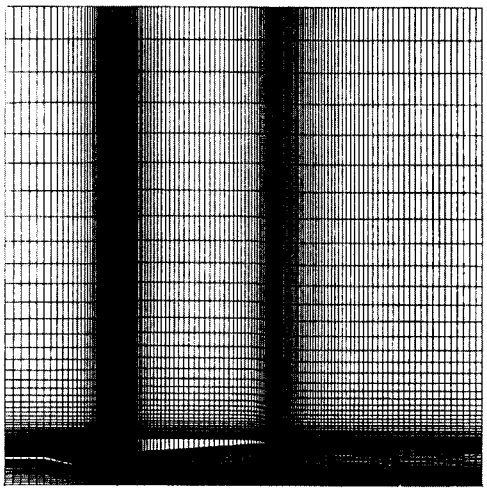

Fig.2 Computational grid for ejector nozzle (171×91).

For all area ratios, the Mach number and pressure contours inside the primary nozzle remain unchanged due to the choking at the exit. For the present calculations, the nozzle pressure ratio exceeds the critical pressure ratio (1.9); thus, the flow beyond the nozzle exit becomes supersonic and results in the formation of a series of shock cells. In the present case, the jet boundary is that of a

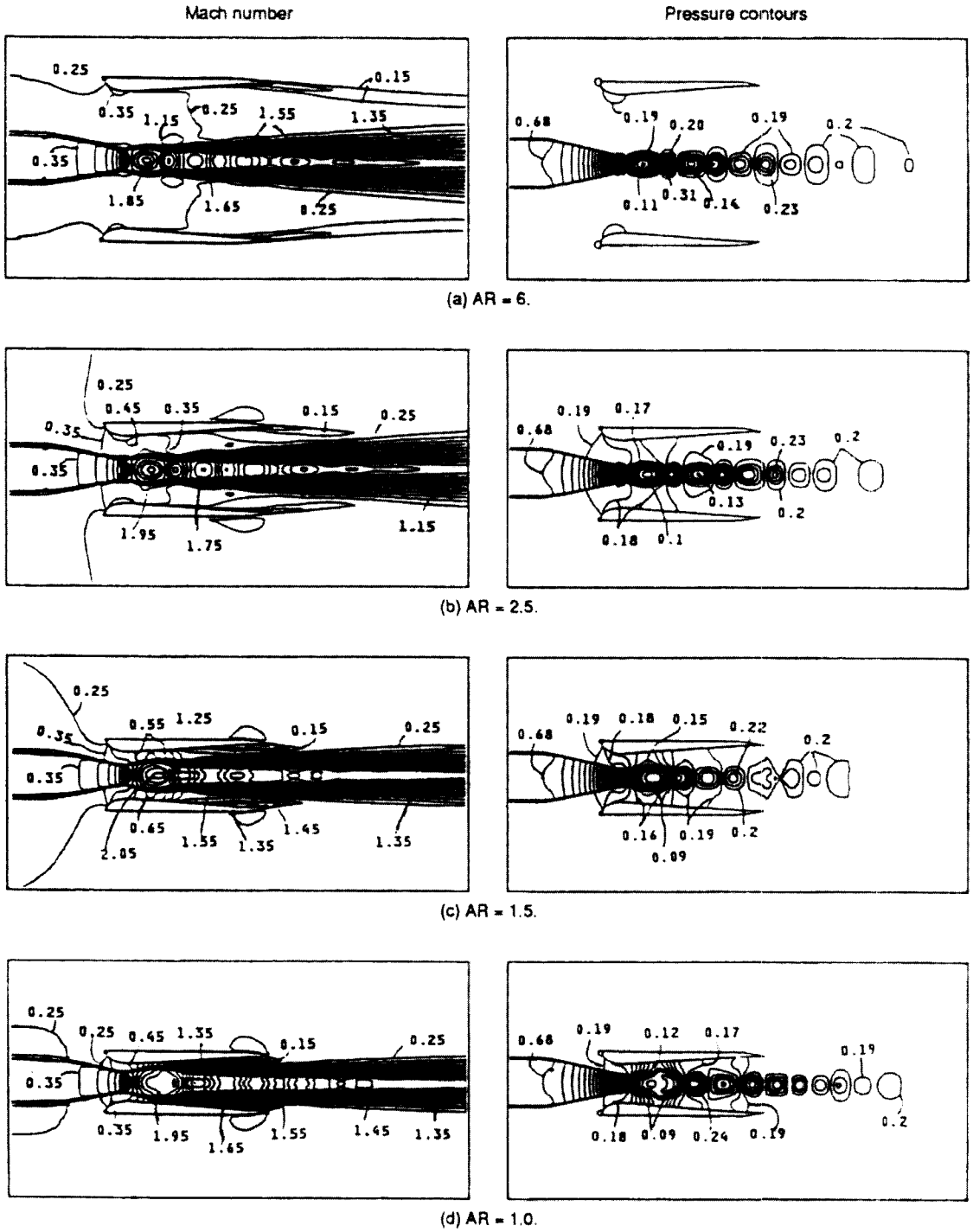

Fig.3 Mach number and pressure contours for area ratios (AR) of 6, 2.5, 1.5, and 2 at a nozzle pressure ratio of 3.5.

constant pressure and the waves reflected on this boundary become waves of the opposite senses (compression waves are reflected as expansion waves). This mechanism forms a shock cell structure in the underexpanded flow. At AR=6, the primary flow expands rapidly at the nozzle exit and becomes a jet with a series of shock cell structures. At the secondary flow passage, however, the Mach number is nearly uniform inside the mixing duct. This suggests that freestream flow is passing directly through the mixing duct; hence mixing between the primary and secondary flows is quite small. The pressure contour also shows nearly uniform pressure through the secondary flow passage. This again indicates uniform flow is passing through without giving efficient pumping.

The results at AR=2.5 are similar to those at AR=6. The Mach number contours in the mixing duct still show the uniform flow region, but the incoming flow is more accelerated due to the effective reduction in the secondary flow area between the shroud wall and the jet boundary. Consequently the rate of the mixing increases. The pressure contour also shows an enlarged low pressure region in the mixing duct inlet region, suggesting more effective pumping.

At AR=1.5, the Mach number changes continuously inside the mixing duct with much faster incoming flow at the mixing duct inlet. Also the pressure contours show that the mixing duct inlet region is dominated by low pressure, which leads to more efficient pumping. However, there is a small separation bubble at the trailing edge region which may deteriorate the thrust performance. This separation occurs because of a very strong adverse pressure gradient (shown later in Fig.5).

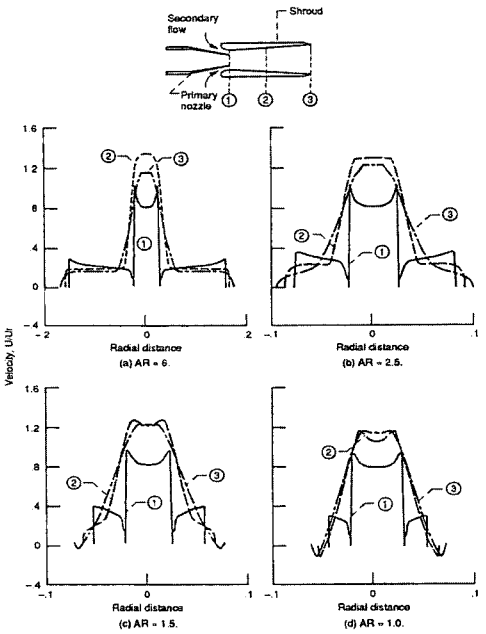

Fig.4 Streamwise velocity profiles for various axial locations and area ratios (AR).

The Mach number contour at AR=1 shows that the jet boundary nearly impinges on the shroud wall. This behavior reduces the effective secondary flow area much less than previous cases and the Mach number increases rapidly. However, it can be noted that the Mach number at the mixing duct inlet is smaller than that when AR=1.5. This suggests that the pumping effect is also smaller for AR=1 than it is for AR=1.5. The reason may be that the jet boundary, which is hitting the shroud wall, blocks the incoming flow. Also the shock cell structure is significantly more distorted than those at larger area ratios. Unlike the previous cases, the jet boundary is no longer at a constant

pressure, and the pressure varies continuously inside the mixing duct as shown in Fig.3. This causes a significant change in the shock cell structure. Pressure contours also show that pressure at the mixing duct inlet is higher at AR=1 than it is at AR=1.5, which again suggests less effective pumping at AR=1.

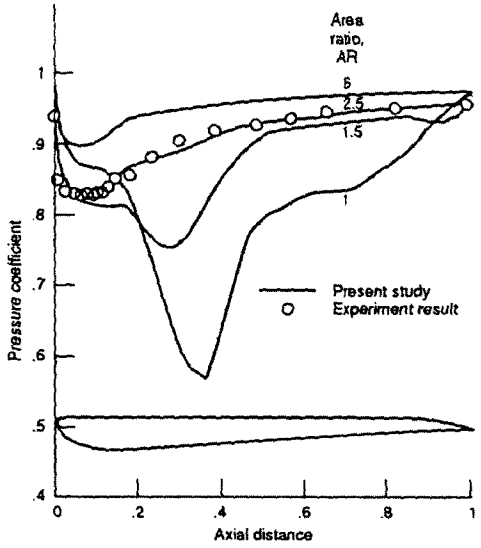

Fig.5 Pressure distribution of the shroud surface. (Area ratio variation)

Some representative streamwise velocity profiles for the above cases are shown in Fig.4. For the four area ratio cases, velocity profiles are presented at the three different axial locations noted in Fig.1. The profile at station 1 is at the exit of the convergent nozzle, and the profiles of stations 2 and 3 are inside the mixing duct region. The streamwise velocity profiles, again, demonstrate the relatively slow rate of mixing between the primary and secondary flows at high area ratios and the increasingly rapid development of flow at the low area ratios. When the velocity magnitudes at the mixing duct inlet section are compared, the average velocity at AR=1.5 is higher than those velocities at other area ratios. This indicates that AR=1.5 is about the optimum shroud position for the pumping capability at this NPR.

The calculated shroud surface pressure distribution is shown in Fig.5. Cases for four different area ratio have been presented. At AR=6 and 2.5, the pressure decreases with downstream distance to reach the minimum near the inlet section of mixing duct; this causes the secondary flow to accelerate in the inlet region. The surface pressure then increases as the flow proceeds downstream until it reaches the ambient pressure at the ejector outlet. At AR=1.5, the pressure distribution along the shroud wall is quite different from that for other area ratios. A large pressure dip is found at about 30% chord length of the shroud after a smooth pressure decrease in the inlet region. At these conditions, the interaction between the shock cell structure of the jet and the shroud wall predominates, which further reduces the secondary flow passage. The pressure dip is attributed to the above interaction phenomena. At AR=1, the pressure dip becomes remarkable. The jet is nearly hitting the shroud wall (refer to Fig.3). This very strong interaction between the jet and the shroud wall greatly decreases the secondary flow passage. Flow acceleration through this passage causes the pressure to drop very quickly. Also the pressure in the mixing duct inlet is higher than it is for the AR= 2.5 and 1.5 cases, suggesting a poor pumping characteristic. The pressure distribution along

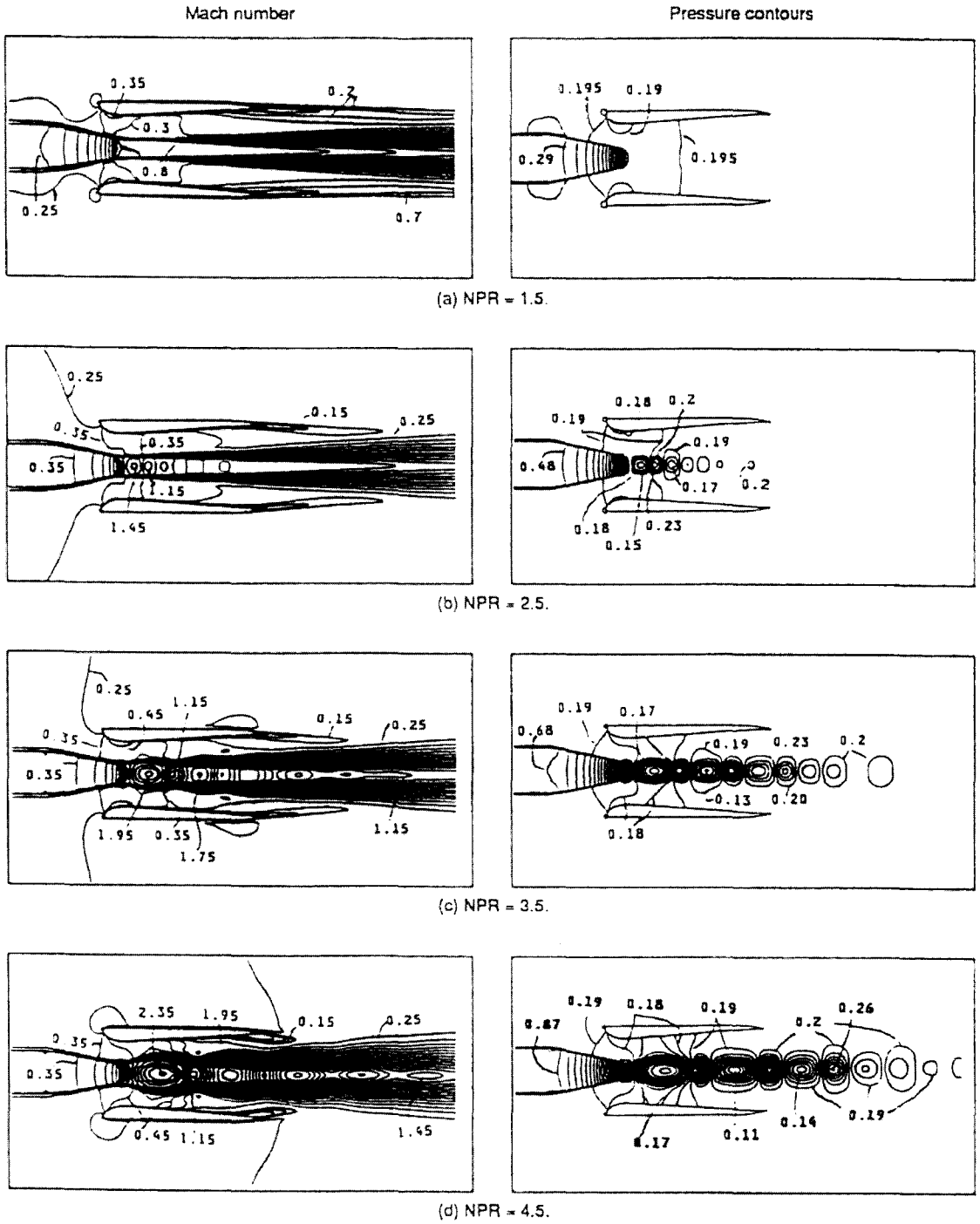

Fig.6 Mach number and pressure contours for nozzle pressure ratios (NPR) of 1.5, 2.5, 3.5, and 4.5 at AR=2.5.

the airfoil shroud wall is compared with experimental data(11) obtained in the 9 by 15 foot low-speed wind tunnel at corresponding area and nozzle pressure ratios (Fig.5). The agreement is quite good at AR=2.5 over most of the shroud wall.

A similar set of calculations is shown in Fig.6 for the case where the nozzle pressure ratio is varied at a constant area ratio. Four nozzle pressure ratio cases have been computed for NPR=1.5, 2.5, 3.5 and 4.5. Corresponding nozzle stagnation pressures are 1.5, 2.5, 3.5 and 4.5 atm, while the ambient stagnation pressure is kept as 1 atm. In all calculations, AR=2.5 is used.

Comparing Mach number contours at various pressure ratios shows that as the nozzle pressure increases, the shock cell structure becomes larger. At NPR=1.5, the shock cell structure does not appear because this pressure ratio is below the critical pressure and the jet is entirely subsonic. At NPR=2.5, the shock cell begins to show up in the vicinity of nozzle exit; at higher pressure ratios, 3.5 and 4.5, the shock cell becomes larger and propagates further into the downstream region. As mentioned before, this large shock cell structure causes reduction in the secondary flow area between the shroud wall and the jet boundary and, therefore, the incoming flow into the mixing duct accelerates as the pressure ratio increases. This suggests more efficient pumping at higher pressure ratios. Also, the jet spreading rate increases as the pressure ratio increases.

Pressure contours are also shown in Fig.6. The development of a shock cell structure can be seen more clearly in these pressure contours. At NPR=1.5, pressure is nearly uniform inside the mixing duct region without any shock cell. But as the pressure ratio increases, the shock cell becomes larger and stronger. In general, we can see that as the pressure ratio increases, the pressure at the mixing duct inlet region decreases. This condition leads to more efficient pumping at higher pressure ratios.

The corresponding pressure distribution on the shroud surface is shown in Fig.7. In general, the pressure at the mixing duct inlet region decreases as the nozzle pressure ratio increases. As mentioned before, this indicates more pumping at higher pressure ratios. At NPR=4.5, however, we see a similar behavior to what was seen at AR=1.5 in Fig.5. The pressure is at a minimum at around 30% of shroud chord length. This occurs because at a high pressure ratio the strong shock cell structure decreases the secondary flow passage and hence the flow accelerates.

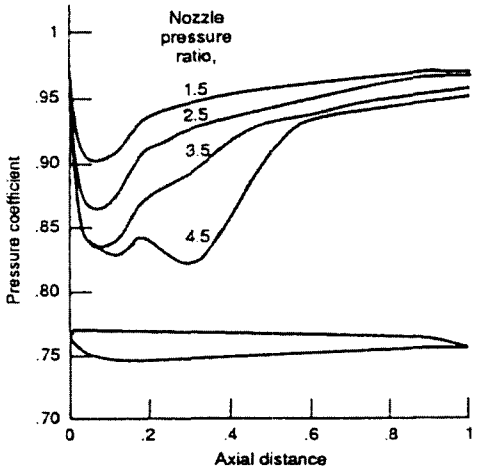

Fig.7 Pressure distribution on the shroud surface. (Nozzle pressure ratio variation)

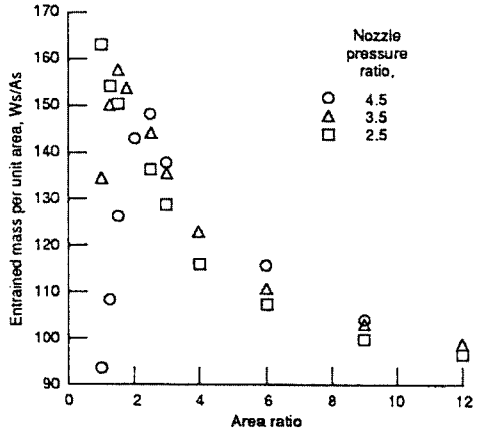

Fig.8 Pumping characteristics of ejector nozzle at various area and nozzle pressure ratios.

The pumping characteristic is an important design parameter of the ejector nozzle for jet noise reduction as well as for ejector performance. Figure 8 shows the pumping characteristic of the ejector nozzle system for various area ratios and nozzle pressure ratios. Computations were made for AR's between 1 and 12 and for NPR's of 2.5, 3.5 and 4.5. The pumping characteristic is expressed in terms of entrained mass flow per unit area (Ws/As). At high area ratios, the pumping characteristic is quite low and approaches a certain asymptotic value. This is because at high area ratios the pumping is negligible and most of the mass flow in the secondary passage is due to freestream flow. But as the area ratio decreases, pumping increases and reaches a peak value, depending on nozzle pressure ratio (At NPR=3.5 the peak pumping rate occurs at about AR=1.5; at NPR=4.5 the peak pumping rate occurs at about AR=2.5; and at NPR=2.5, the pumping rate increases until AR=1 is reached.) A poor pumping characteristic is seen for very low area ratios at NPR = 3.5 and 4.5 because of the blocking effect caused by the shroud wall and the shock cell structure interaction. It is also anticipated that there is a certain area ratio for NPR=2.5 where pumping will be reduced.

6. Summary

A time-iterative compressible Navier-Stokes code is developed to analyze the flowfield of a two-dimensional ejector nozzle. The numerical method employs an Euler implicit discretization in time along with central differencing in space for both the inviscid and viscous terms. A computational study of the flowfield in a two-dimensional ejector nozzleshows that the flow feature inside the ejector nozzle is complicated by strong inviscid/viscous interaction, freestream entrainment, shock cell structure, and the presence of both supersonic and subsonic flow regions. A parametric study has been made for two controlling parameters, duct to nozzle area ratio and nozzle pressure ratio. Results show that there is an optimum area ratio for an efficient pumping of secondary flow. At high area ratios, the freestream flow passes directly through the mixing duct without providing adequate pumping. At low area ratios, the jet boundary blocks incoming flow. The nozzle pressure ratio variation shows that pumping rate increases as the pressure ratio increases provided there is no interaction between the shroud wall and the shock cell structure (i.e. for a certain area ratio). The comparison with experimental data also shows quite good agreement.

References

1. Seiner, J. M., and Krejsa, E. A., "Supersonic Jet Noise and the High Speed Civil Transport," AIAA paper 89-2358, 1989
2. Presz, W. M. Jr., Morin, B. L., and Gousy, R. G., "Forced Mixer Lobes in Ejector Designs," Journal of Propulsion and Power, Vol.4, No.4, 1988, pp.350-355
3. Presz, W. M. Jr., Blinn, R. F., and Morin, B. L., "Short Efficient Ejector Systems," AIAA paper 87-1837, 1987
4. Tillman, T. G., Paterson, R. W., and Presz, W. M. Jr., "Supersonic Nozzle Mixer Ejector," AIAA paper 89-2925, 1989
5. Von Karman, T., "Theoretical Remarks on Thrust Augmentation," Riessner Anniversary Volume, edited by J. W. Edwards, University of Michigan Press, Ann Arbor, 1949, pp.461-468
6. Porter, J. L. and Squyers, R. A., "An Overview of Ejector Theory," AIAA paper 81-1678, 1981
7. Deese, J. E. and Agarwal, R. K. H., "A Numerical Study of Viscous Flow in Inlets and Augmentors," AIAA paper 88-0187, 1988
8. Baldwin, J. S. and Lomax, H., "Thin Layer Approximation and Algebraic Model for Separated Turbulent Flows," AIAA paper 78-257, 1978
9. Pulliam, T. H. and Steger, J. L., "Implicit Finite Difference Simulation of Three Dimensional Compressible Flow," AIAA Journal, Vol.18, No.2, 1980, pp.159-167
10. Jameson, A., Schmidt, W., and Turkel, E., "Numerical Solutions of the Euler Equations by Finite Volume Methods Using Runge-Kutta Time-Stepping Schemes," AIAA paper 81-1259, 1981
11. Whitehead, A. H. Jr., "The First Annual High-Speed Research Workshop Proceeding," NASA CP 10087, 1992